JOTCS A
Journal of the Turkish Chemical Society
Section: A
Chemistry
TURKISH CHEMICAL SOCIETY

Isotherm and Thermodynamic Studies on the Removal of Gelatin-Stabilized Silver Nanoparticles from Water by Activated Carbon

Aysenur Ceryan[1], Nurettin Eltugral[2*]

[1]Bolu Abant Izzet Baysal University, Department of Property Protection and Security, Bolu, 14030, Turkey
[2]Karabük University, Department of Medical Engineering, Karabük, 78050, Turkey.

Abstract: Gelatin-stabilized silver nanoparticles (AgNPs) with a particle size of 6.9 (±3.2) nm were synthesized and employed in nanoparticle adsorption onto activated carbon (AC). Subsequently, the synthesized AgNPs and the adsorbed nanoparticles onto the AC (AgNP@AC) were characterized by various techniques including UV–Vis spectrophotometry, transmission electron microscopy (TEM), scanning electron microscopy (SEM), Fourier transform infrared spectroscopy (FT–IR) and X–ray diffraction (XRD). AgNPs possessed colloidal stability at a wide pH interval ranging between 4 and 13. Adsorption was studied batch-wise as a function of initial nanoparticle concentration (4–14 mg L^{-1}), temperature (298–323 K), pH (4–13) and adsorbent dosage (0.01–0.05 g). Adsorption isotherms were investigated by fitting the data to different isotherm models including Langmuir, Freundlich, Temkin, and Dubinin–Radushkevich (D–R). Error analysis indicated that the adsorption is well described by the Langmuir model with a monolayer adsorption capacity of 10.36 mg g^{-1} for 0.05 g AC at pH 7 and 323 K. Thermodynamic parameters such as enthalpy (66.77 kJ mol^{-1}), entropy (232.92 J mol^{-1} K^{-1}), and Gibbs free energy (–8.31 kJ mol^{-1}) indicated that the process is endothermic, favorable and spontaneous through physical interactions.

Keywords: Adsorption, silver nanoparticles, activated carbon, adsorption isotherms, thermodynamic parameters.

Submitted: April 14, 2022. **Accepted:** July 12, 2022.

Cite this: Ceryan A, Eltugral N. Isotherm and Thermodynamic Studies on the Removal of Gelatin-Stabilized Silver Nanoparticles from Water by Activated Carbon. JOTCSA. 2022;9(3):919–38.

DOI: https://doi.org/10.18596/jotcsa.1098891.

***Corresponding author. E-mail:** nurettineltugral@karabuk.edu.tr.

INTRODUCTION

Silver nanoparticles (AgNPs) have been a focus research field by scientists from different disciplines due to their unique properties which has opened new capabilities in a wide range of applications (1). Silver nanoparticles (AgNPs) have already been utilized in many fields including medical equipments, textile industry, water treatment, ventilation and air conditioning systems, cosmetics, and sport equipments as they possess high antibacterial activity (2,3).

Nano-silver can be prepared according to a common method which involves wet chemical synthesis where a silver salt precursor is reduced in the presence of a stabilizer (3). The most commonly considered agents for reducing silver salt are sodium borohydride ($NaBH_4$) (4), citrate (5), ascorbic acid (6), dimethylformamide (DMF) (7,8), and oleylamine (9).

Colloidal instability of AgNPs against aggregation has been encountered as a common problem for many applications. This problem may end up with the formation of large aggregates which causes the blockage of the active surface area, thus limiting the unique antibacterial and catalytic properties (3). Therefore, to avoid this problem and improve colloidal stability as well as the availability of AgNPs for further applications, their surface is needed to be protected. For this purpose, there are many types of chemicals such as surface-active agents which are also called surfactants (10,11), synthetic polymers,

i.e. polyvinyl pyrrolidone (PVP) (12), polyvinyl alcohol (PVA) (13), polyethylene glycol (PEG) (14), polymethyl methacrylate (PMMA) (15), and dendrimers (16). Additionally, natural polymers such as chitosan (17,18), polysaccharides, and gelatin are potentially preferred for the stabilization of AgNPs (19–22). These ligands prevent nanoparticles from being aggregated in the surrounding atmosphere and are also heavily important in determining the particle size and shape in colloidal systems (23,24).

Activated carbons (ACs) have a relatively porous structure and large surface area, which can act as a host structure, as well as they consist of amines, phenols, nitrobenzene, and other types of cationic functional groups on its surface. The adsorption capacity of ACs can be estimated based on these chemical functionalities. The incorporation of silver nanoparticles onto ACs has gained a greater choice of interest for use as the host material in wastewater treatment, air purification, and removal of organic and inorganic contaminants (25,26).

In a previous report, adsorption of AgNPs modified by using different types of ligands onto AC was studied to investigate the ligand type on the adsorption performance (27). Since ligands are surrounding the active metal surface, they play an important role in nanoparticle interaction with the outside world. Gelatin is an excellent coating material to produce nanoparticles that show high endurance and stability in a wide range of pH. Since gelatin-stabilized nanoparticles could can a long-term aggregation resistance in aqueous media including natural aquatic ecosystems, their removal from wastewaters might be challenging and this appears to be a scientific concern. Therefore, in this study, it is aimed to investigate the adsorption of gelatin-stabilized AgNPs onto AC. In that regard, gelatin-stabilized AgNPs were synthesized and employed in nanoparticle adsorption onto AC. Batchwise adsorption studies were conducted between AgNPs and the AC as a function of initial nanoparticle concentration (4–14 mg L^{-1}), temperature (298–323 K), pH (4–13), and adsorbent dosage (0.01–0.05 g). Adsorption isotherms were investigated by fitting the data to different isotherm models including Langmuir, Freundlich, Temkin, and Dubinin–Radushkevich (D–R). The resulting nano–silver–AC product (AgNPs@AC) was characterized by several techniques including UV–vis, TEM, SEM, XRD, and FTIR.

EXPERIMENTAL SECTION

Materials and methods

Silver nitrate ($AgNO_3$, 99.0%), sodium borohydride ($NaBH_4$, 98.0%), ammonia (NH_3, 25–30%), sodium carbonate (Na_2CO_3), and gelatin were purchased from Sigma-Aldrich. NaOH, HCl (37%), $NaHCO_3$, phenolphthalein, and methyl orange were purchased from Merck. AC was purchased from Nanografi. All reagents were of analytical grade and used as received. Ultrapure water was used for the preparation of all samples during the experiments.

The pH of the samples was adjusted using a Mettler Toledo model pH meter by adding either 0.1 M HCl or NaOH. The prepared AgNPs colloids were checked for their optical properties and long-term stability by collecting absorbance spectra on a double beam UV–vis spectrophotometer (Agilent Cary 60 UV–vis Spectrophotometer). All the spectra were recorded between 700 and 300 nm. The crystal structure of the prepared samples were analyzed through the X–ray diffraction (XRD by Rigaku). Morphology of the synthesized nanoparticles was studied using a transmission electron microscope (TEM by Jeol 2100F RTEM 200 kV). Structural and morphological properties of AgNPs@AC was investigated through a SEM device (by Carl Zeiss Ultra Plus Gemini FESEM at accelerating voltage in the range of 5–10 kV, equipped with an energy-dispersive X–ray (EDX) spectrometer). Identification of organic groups were performed on a FTIR spectrometer (FTIR by Bruker Alpha Platinum FTIR–ATR spectrometer equipped with a single reflection diamond ATR accessory). X-ray and FT–IR analysis of the AgNPs were done on the solid powder form of the product by evaporating its water content.

Synthesis of Silver Nanoparticles

Silver nanoparticles were synthesized according to the Tollens' method (28). Accordingly, aqueous solutions of $AgNO_3$ (20 mL, 2.5×10^{-3} M), NH_3 (20 mL, 1.25×10^{-2} M), and NaOH (10 mL, 5×10^{-2} M) were mixed thoroughly under constant stirring to obtain $[Ag(NH_3)_2]^+$ complex under basic conditions. Then, 2.5 %(w/w) 1.25 gr of gelatin was added and finally, a freshly prepared aqueous solution of $NaBH_4$ (5 mL, 0.1 M) was added dropwise yielding a yellow-brownish color of solution which indicated the AgNPs formation. The resulting mixture was further stirred for 20 min at ambient temperature and kept dark throughout the experiments. The pH of the prepared stock nanoparticle solution was measured to be 11.5. Nanoparticle molar concentration was expressed in terms of silver content and it was 9.1×10^{-4} M (98 mg L^{-1}) for the stock nanoparticle solution. A representative absorbance spectrum of a diluted nanoparticle solution (1.8×10^{-4} M) was given in Figure 1(a).

Identification of surface groups of the AC

Bohem titration method (29) was employed for characterizing the surface functional groups and the acidity of the AC as described in our previous work (27). In this regard, 0.1 g of the AC was mixed with NaOH, $NaHCO_3$, and Na_2CO_3 (each, 50 mL, 0.1 N), respectively, and agitated for 36 h at room temperature. Then, carbon was filtered off and 10 mL of each supernatant was titrated with 0.1 N HCl in the presence of phenolphthalein and methyl orange indicators. Thus, acidic groups on the AC was calculated. NaOH neutralizes carboxylic, lactonic, and phenolic groups, Na_2CO_3 neutralizes carboxylic and lactonic groups, and $NaHCO_3$ neutralizes

carboxylic groups present on the AC. Similarly, 1 g of the AC was mixed with 0.1 N HCl (50 mL, 0.1 N) and agitated for 36 h at room temperature to determine total basicity. Then, 10 mL of the supernatant was titrated against 0.1N NaOH to calculate the number of basic groups.

Adsorption Studies

In the present study, 10-mL solutions of AgNPs, each having a concentration and a pH in the range of 3–15 mg L^{-1}, and 4–12, respectively were prepared by diluting the stock AgNPs to the proper concentration and changing the pH (4, 7, 10 and 12) with 0.1 M HCl or NaOH. To each of the prepared nanoparticle solution, 0.05 g of AC was added and agitated at room temperature for 24 h of equilibrium contact time at a low rpm. After that, the supernatant was first filtered off through a filtering paper (M&Nagel–125 mm) followed by a syringe filter (0.45 µm pore size). The supernatant liquids were checked for their nanoparticle content by collecting absorbance spectra at a wavelength of 415 nm. The same procedure was employed to study the effect of temperature and adsorbent dosage.

The nanoparticle concentrations (in silver content) were determined by plotting a calibration curve by recording the absorbance for diluted nanoparticles samples of known concentrations having absorbance in the range of 0.1–0.5 at a wavelength of 415 nm. The adsorbed nanoparticle concentration (q_e, mg g^{-1}) on the AC was calculated using the following equation;

$$q_e = \frac{(C_o - C_e)V}{m} \quad (1)$$

Where C_o is the initial concentration of AgNPs, C_e (mg L^{-1}) is the equilibrium concentration of the nanoparticles in the aqueous phase, V (L) is the volume of the solution, m (g) is the mass of AC@AgNPs, and q_e (mg g^{-1}) is the calculated amount of nanoparticle concentration adsorbed onto the AC. Additionally, the percent adsorbed amount *(%R)* was obtained by the equation:

$$\%R = \frac{(C_o - C_e)}{C_o} x\,100 \quad (2)$$

RESULTS AND DISCUSSION

Characterization of silver nanoparticles

Silver nanoparticles were synthesized according to the Tollens' process (28). This process is based on the reduction of silver complex, $[Ag(NH_3)_2]^+$ in alkaline media using suitable reducing agents. In our study, sodium borohydride ($NaBH_4$) was used as a reducing agent. $NaBH_4$ is one of the most powerful reducing agents used in nanoparticle synthesis. For example, its reduction of power is large enough to reduce iron salts to iron nanoparticles (30). Gelatin, a natural polymer, was used as a stabilizer to protect the highly active metal surface at the nanoscale.

Figure 1(a) shows the UV–vis absorption spectra obtained after diluting the stock nanoparticle solution. AgNPs exhibits a narrow absorbance band at 415 nm as a result of surface plasmon resonance (31). Silver nanoparticles of spherical shape have a characteristic absorbance band 410 and 430 nm with an average particle size of 6 and 30 nm, respectively (3,32). A representative TEM image of nanoparticles is shown in Figure 1(b). The average particle size calculated from TEM results is 6.9 (±3.2) nm. Our findings from TEM analysis were in good agreement with UV analysis.

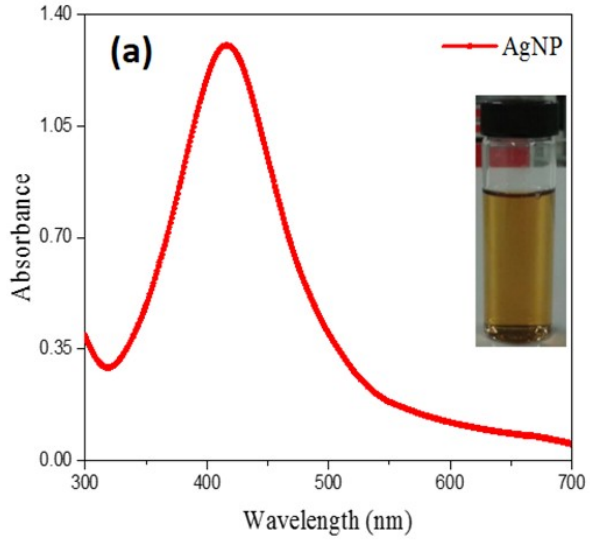

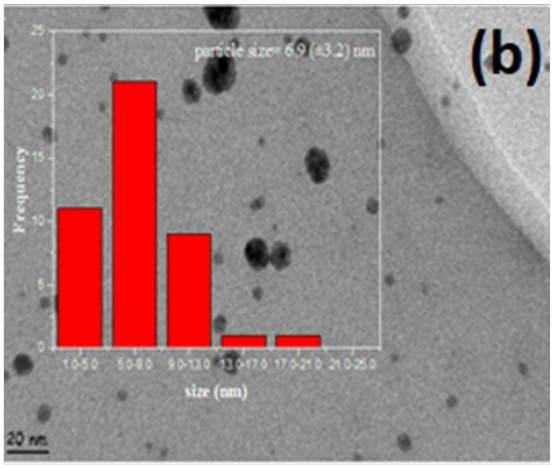

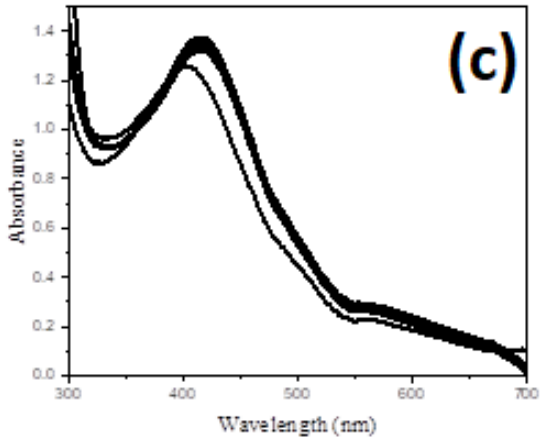

Figure 1: (a) UV–vis spectrum of gelatin-stabilized AgNPs (1.8×10^{-4} M); inset is a photo of nanoparticle solution, (b) TEM and size distribution histogram of the synthesized nanoparticles and (c) AgNP UV–vis spectra at different pH values.

Spectrophotometric investigations show that AgNPs are stable over months as reported previously (33). The extinction coefficient of 7171.9 M^{-1} cm^{-1} at the wavelength of 415 nm was obtained as the slopes of absorbance vs concentration plots (see supplementary information, Figure S1((a) and (b)). As it can be understood from the linearity of the plot and the correlation coefficient value≈1, it shows that the absorbance values of different concentrations of AgNP at 415 nm give good correlations with the Lambert–Beer law (34,35).

The influence of gelation on the colloidal stability of the AgNPs was investigated against the pH. For this purpose, the pH of diluted AgNPs solutions was adjusted to different pH values (2, 5, 7, 9, 11, and 13) by adding either 0.1 M HCl or 0.1 M NaOH. Then absorbance spectra of the resulting samples were recorded. Figure 1(c) shows that AgNPs exhibits similar absorbance spectra over a wide range of pH except pH 2.

Nitrogen atoms of the amine groups in gelatin covalently interact with the metal surface and attach themselves to the metal core thus stabilizing the nanoparticle. Gelatin can have different charges at different pH values owing to the carboxylic and amine groups in its structure. In the acidic media, amine groups are positively charged while carboxyl groups remain the same. At high pH values, carboxyl groups lose the hydrogen and become negatively charged while amine groups remain the same. Since the carboxyl groups of gelatin become negatively charged, the nanoparticle surface gains a negative charge as well, thus preventing the particles from interacting with each other by electrostatic repulsion. However, at low pH values, amine groups that interact with the metal in the acidic environment become positively charged. Although, the covalent interaction between the nitrogen atom and the metal surface is impaired, this time it is expected that gelatin surrounds and stabilizes the metal core as a result of the electrostatic interaction between the positively charged amino groups and metal's surface electrons. A proposed model for gelatin-stabilized AgNPs under acidic or alkali media is shown in Fig. 2.

When the carboxyl groups do not carry a net charge, there will be no electrostatic repulsion between the particles, which can cause the particles to interact with each other and collapse in the solution by forming aggregates. The sudden change in the absorbance profile of AgNPs at pH 2 is attributed to the aforementioned effect, inconsistent with the result in the literature (3).

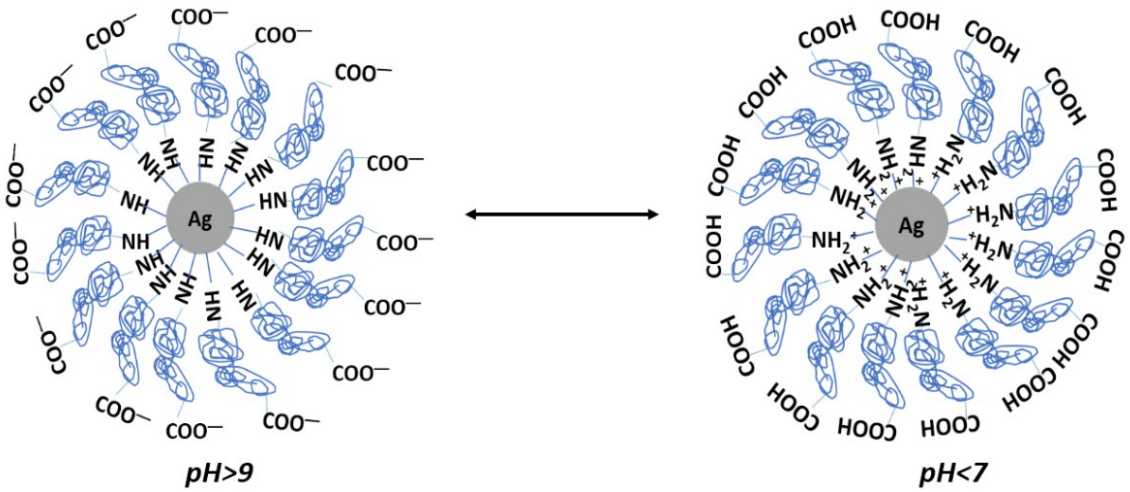

Figure 2: A schematic model for gelatin-stabilized AgNPs under acidic and basic media.

Gelatin is an amphiphilic molecule and the isoelectric point for gelatin is approximately 8.5 (between 7–9) (36). This means that the negative and positive charges on the molecule are in balance between the pH of 7 and 9. The presence of negative charges on the surface ensures that the nanoparticles are colloidally stable against aggregation and precipitation. Colloidal stability lasts as long as there exists a negative charge on the particle surface over a pH range.

Characterization of AgNPs@AC

Figure 4 shows an SEM image of AgNPs adsorbed onto the surface of AC. The SEM image shows that AgNPs are deposited on the entire surface of the AC with sizes range between 50–140 nm. The nanoparticle surface is coated with gelatin which mainly regulates the interaction between the nanoparticle and adsorbent (32). Therefore, it is claimed that gelatin functional groups can interact with the surface functional groups of AC during the formation of AgNPs@AC.

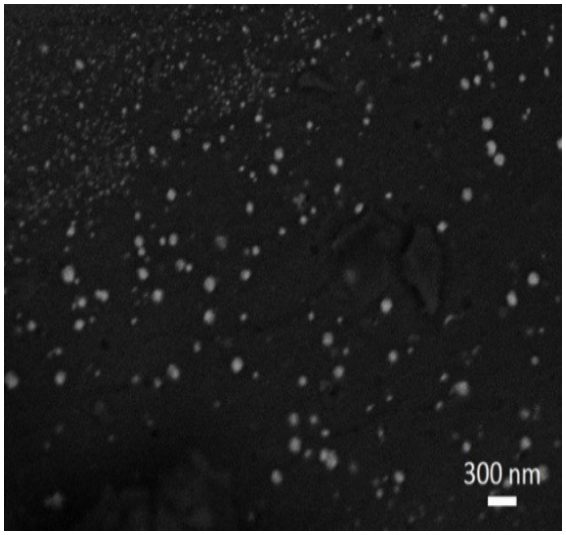

Figure 3: SEM image of AgNP@AC.

The functional groups of the sole AgNPs and AgNPs@AC were examined using FTIR spectra (see Figure S2). First of all, when the IR spectrum of gelatin is examined, the peak between 3400–3200 cm^{-1} is assigned to the peptide bond by N–H stretching, whereas, the peak around 3100–2800 cm^{-1} corresponds to C–H stretching. The peak 1660–1600 cm^{-1} is assigned to the stretching of C=O attached to peptide unit. Two peaks around 1565–1500 cm^{-1} and 1450–1300 cm^{-1} can be attributed to C–N–H and C–H bending of the amino group of gelatin. (37). AgNPs possess a similar FTIR spectrum to that of gelatin except for peak intensities, and the band between 3400–3200 cm^{-1} is observed to broaden. We attribute the observed broadening to be the consequence of the interaction of peptide

amine groups with the active metal surface. Besides, FTIR of AgNPs does not display a new peak other than that of gelatin which indicates no chemical bonding occurs between gelatin and silver atoms (38).

For the functional groups of AC, a broad peak positioned between 2500–3000 cm^{-1} indicates the stretching vibrations of the –OH on the carboxyl group while the peak centered at 1500–1330 cm^{-1} is designated to C=C stretching of aromatic rings. The peak at 1000–1180 cm^{-1} could be attributed to C–O stretching.

When AgNPs were doped on the AC, nanoparticles could be traced in the FTIR spectrum by observing the N–H band of the gelatin stabilized–AgNPs that appeared between 1500–2000 cm^{-1}. The intensity of the FTIR peaks of the AgNPs seemed to decrease. These findings indicate that AgNP was successfully adsorbed to the AC surface.

The XRD patterns of AgNP, AC and AgNP@AC are shown in Figure S3. XRD pattern of AgNP shows major characteristic peaks with 2θ values 37.3º, 43.5º, 64.8º, and 77.3º which are assigned to (111), (200), (220), and (311) lattice planes of the face-centered cubic structure of metallic Ag (39–41). The broad and reduced intensity of peaks that the diffractograms displayed are due to smaller particle size and high concentration of the gelation layer at the surface of the metallic core (42). AC has a broad XRD pattern without any sharp and intense peaks since it is an amorphous structure (43,44). AgNP@AC yielded almost the same XRD pattern as that of AgNPs which means that there is no significant change in AgNPs (44,45).

Table 1 summarizes the amount of functional surface groups of AC using the Boehm titration method. The obtained data show that AC has both basic and acidic properties (46). Acidic groups such as phenol and carboxyl are not expected to release their acidic protons under acidic pH values. However, basic surface groups such as amine, chromene, and pyrene are protonated and the carbon surface can have a positive charge. A negative charge on the carbon surface may refer to the decomposition of acidic regions such as carboxyl and phenol, which release their protons under basic pH conditions (47).

Table 1: Amount of groups on the surface of activated carbon.

Surface Groups (meq g^{-1})					
Sample	Carboxylic	Lactonic	Phenolic	Acidic	Basic
Activated carbon	0.400	0.550	2.150	3.100	0.300

Effect of AgNP initial concentration and temperature

The effect of initial AgNP concentration and temperature on the efficiency of its adsorption onto 0.05 g AC was investigated by varying the initial concentration at 298, 308, and 323 K, and the results are shown in Figure 8. The percentage amount of AgNP adsorbed on the AC was observed to decrease with increasing nanoparticle concentration (Figure 4(a)). When the amount of AC is fixed, the decrease in the adsorption percentage is probably due to the saturation of the active binding sites on the AC surface at higher AgNP concentrations. However, the amount of AgNP adsorbed per AC unit mass (q_e) was observed to increase as the AgNP concentration increases (Figure 4(b)). AgNP concentration provides an important driving force to overcome mass transfer resistance for AgNP transfer between nanoparticle solution and AC surface (48,49). In this process, AgNP first encounters the AC boundary layer. It then diffuses to the AC boundary surface layers and subsequently into the pores. Additionally, an increase in percentage adsorption occurred with an increase in temperature.

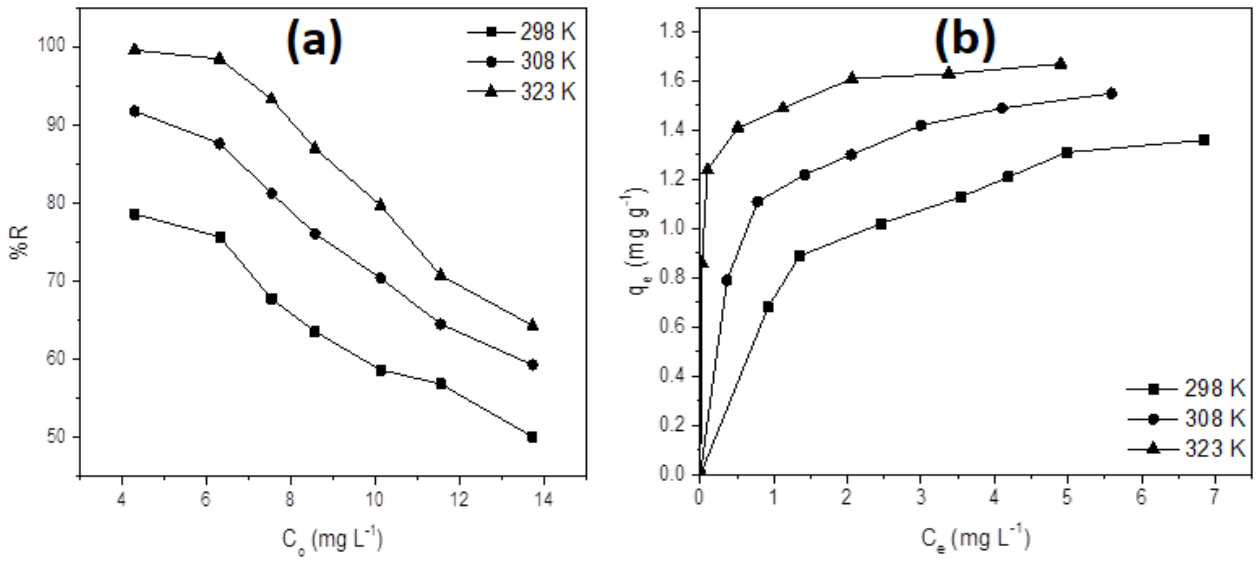

Figure 4: (a) Effect of initial nanoparticle concentration, and (b) temperature on the AgNP@AC adsorption (AgNP concertation: 4–14 mg L^{-1}, pH 7, AC dosage: 0.05 g).

The temperature increase was observed to promote AgNP adsorption, which is typical for endothermic adsorption. The increase in AgNP adsorption with temperature can be explained by the increase in the AgNP mobility thus increasing the number of active binding sites on the AC surface for adsorption as a result of the enlargement of the AC pores (50).

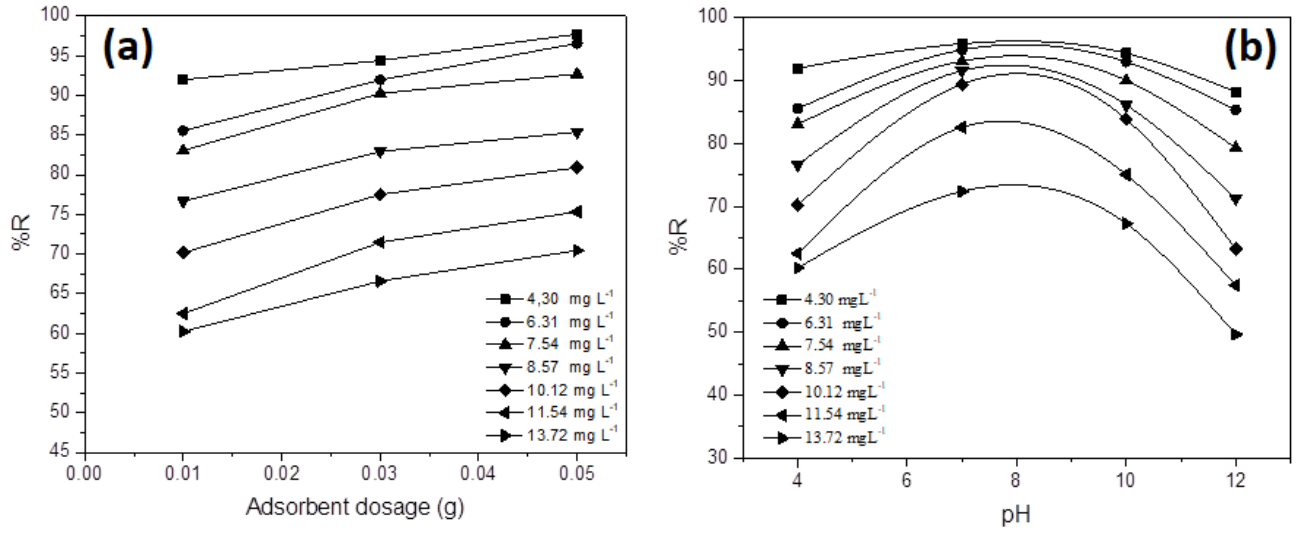

Figure 5: (a) Effect of dosage on AgNP@AC adsorption (AgNP concentration: 4–14 mg L^{-1}, pH 7, 298 K) (b) Effect of pH on AgNP@AC adsorption (AgNP concentration: 4–14 mg L^{-1}, AC dosage: 0.05 g, 298 K).

Effect of Adsorbent Dosage

The amount of adsorbent is an important factor in determining the capacity of the adsorbent for a certain concentration of AgNP solution in adsorption studies (50). AgNP@AC adsorption was investigated as a function of AC dose for AgNP in the concentration range of 4.30–13.72 mg L^{-1} and the results are given in Figure 5 (a). It was observed

that the adsorption capacity increased after the dosage of the adsorbent is increased due to the greater accessibility of surface binding sites with an increased dosage of the adsorbent. This can be explained by increasing of the available sites with increasing adsorbent dosage for the interaction with the AgNP in solution and lead to increases in the removal efficiency of the nanoparticles. On the other hand, the amount of AgNP adsorbed per unit mass of AC has decreased as the adsorbent dosage increased (51).

Many factors affect adsorption by increasing the amount of adsorbent. The first and most important factor is that the binding sites remain unoccupied without any saturation during the adsorption. This is because as the amount of adsorbent increases, there is less increase in adsorption resulting from the lower adsorptive capacity utilization of the adsorbent (52). The second factor is the aggregation of sorbent particles at higher doses, which leads to a decrease in surface area and an increase in the diffusion path length. Finally, the third factor, particle interactions at high sorbent dosages may cause some of the loosely bound AgNP to desorb from the AC surface (53).

Effect of pH

The nanoparticle surface functional groups, as well as the AC surface nature, can be very sensitive to the solution pH, and therefore, it can directly affect the surface binding during the adsorption process (28). In this study, the effect of pH was investigated in the range of 4–12, at room temperature, for the nanoparticle concentration range of 4.30–13.72 mg L^{-1} for 0.05 g of AC. The results shown in Figure 5(b) suggest that the pH of the solution significantly alters the adsorption. The pH dependence of adsorption can be explained by the isoelectric point, pH_{IEP} that is the pH at which a molecule carries no net charge (50).

pH_{IEP} can be used as an index for positive or negative loading capability and can be controlled according to the pH of the solution. This phenomenon is basically due to the presence of functional groups present on both the nanoparticles and the activated carbon. Those functional groups show different ionization/dissociation by the influence of the pH. Namely, if the solution pH is lower than pH_{IEP}, the sorbent surface acts as a positive surface, and vice versa. Besides, the observed pH effect is also closely related to AgNP surface chemistry (54).

The pH_{IEP} for AgNP solution is in the range of 7–9, and it is in the range of 2–3 for the studied AC. Accordingly, in the adsorption process, which takes place at pH 4 and 7 AgNP is well adsorbed to the AC surface since the AgNP surface was negative while the AC surface was positively charged. When the pH of the medium was in the range of 7–10, AgNP has partially negative and positive charges on its surface due to its pH_{IEP} value. When pH shifts towards 10, the amount of nanoparticle uptake decreases due to the decrease of electrostatic attraction forces. Finally, strong repulsive electrostatic forces from the surfaces at pH 12, where both AgNP and AC surface are negative, also decreases the adsorption (55). But hydrophobic interactions provide an important driving force for AgNP uptake onto the AC surface (55).

Adsorption Isotherms

Adsorption isotherms are widely utilized methods while studying the equilibrium of the adsorption. Various isotherm equations have been derived to determine adsorption properties and understand the driving forces behind the process. Four important models of Langmuir, Freundlich, Temkin, and Dubinin–Raduskevich (D–R) isotherms derived from the equations were applied to this study.

Langmuir isotherm

Langmuir isotherm is based on the assumption that the adsorption process takes place in certain homogeneous regions on the adsorbent, that when AgNP is attached somewhere on the AC surface, no further adsorption can occur in that region, and the adsorption process is single-layered (56). Experimental data were evaluated with Langmuir isotherm to determine whether the adsorption event is a monolayer. Langmuir isotherm is expressed by the linear equation given below;

$$\frac{C_e}{q_e}=\frac{1}{K_L q_m+\frac{1}{q_m}}C_e \qquad (3)$$

where; q_m is the maximum amount of absorption (mg g^{-1}), q_e is the amount of substance at equilibrium (mg g^{-1}), K_L is the Langmuir equilibrium constant (L mg^{-1}), C_e is the nanoparticle concentration remained in solution at equilibrium (mg L^{-1}) (57). Besides, the further characteristics of Langmuir isotherm can be described by a factor, separation factor, which is defined by the following equation

$$R_L=\frac{1}{1+K_L.C_e} \qquad (4)$$

The R_L value indicates the nature of the adsorption which is favorable when $0<R_L<1$.

Freundlich Isotherm

The Freundlich isotherm equation used to describe the multi-layered adsorption systems of the adsorption process is shown linearly as follows (57).

$$lnq_e=lnK_f+ln\frac{1}{n}C_e \qquad (5)$$

Where K_f (L g^{-1}) is the Freundlich absorption constant related to adsorption capacity and

represents the quantity of nanoparticle adsorbed onto the adsorbent. q_e is the amount of substance adsorbed per unit of adsorbent at equilibrium (mg g^{-1}), n is Freundlich absorption constant, and for $n > 1$ a physical adsorption is favored. Furthermore, the *1/n* value indicates the heterogeneity and ranges between 0 and 1. For heterogeneous surfaces, this value approaches 0 (58).

Temkin Isotherm

In an absorption process, the heat of absorption and indirect adsorbent-adsorbate interactions were studied by Temkin and Pyzhev. The Temkin isotherm equation is given as

$$q_e = B \ln\left(K_T\right) + B \ln\left(C_e\right) \quad (6)$$

$$B = \frac{RT}{b_T} \quad (7)$$

Where K_T is the equilibrium binding constant (L g^{-1}) of the Temkin isotherm, b_T is the Temkin isotherm constant, R is defined as the ideal gas constant (8.314 J mol^{-1} K^{-1}), and B is defined as the adsorption heat constant (J mol^{-1}) (59).

Dubinin–Radushkevich (D–R) isotherm

Dubinin–Radushkevich isotherm is generally used to express the adsorption mechanism on a heterogeneous surface with Gaussian energy distribution (60). The relation expressing this isotherm is shown in eq. (8) (61).

$$\ln q_e = \ln q_s + \left(K_{DR}\right) + \mathcal{E}^2 \quad (8)$$

Where, q_e is expressed as equilibrium adsorbent amount (mg g^{-1}), q_s is adsorption saturation capacity (mg g^{-1}), K_{DR} Dubinin-Radushkevich isotherm constant related to the adsorption energy (mol^2 J^2), $\mathcal{E}$ Dubinin-Radushkevich constant (61). This constant can be expressed as

$$\mathcal{E} = RT \ln\left(1 + \frac{1}{C_e}\right) \quad (9)$$

where; R represents the ideal gas constant (8.314 J mol^{-1} K^{-1}), T is absolute temperature (K), C_e is adsorbent equilibrium concentration (mg L^{-1}) (61).

This approach can usually be calculated by the following correlation with the mean free energy, E for adsorption, and the E value gives information on whether the adsorption is chemical or physical (61).

$$E = \sqrt{\frac{1}{2K_{DR}}} \quad (10)$$

If E value is less than 8 kJ mol^{-1}, the interaction between adsorbate-adsorbent is physical. If on the contrary, it is greater than 8 kJ mol^{-1}, adsorption refers to a chemical interaction (62).

Langmuir, Freundlich, Temkin, and Dubinin-Radushkevich isotherms of AgNP@AC adsorption processes at different pHs (4,7,10 and 12) are shown in Figure 6. Also, isotherms were carried out at different temperatures and adsorbent amounts. Isotherm parameters and correlation coefficients (R^2) obtained from the plots are summarized in Tables 2 and 3. The Langmuir isotherm parameters, K_L, and qm were obtained from the slope and intercept respectively from the plot shown in Figure 6 (a). The compatibility of experimental data was also evaluated by applying different temperatures and AC amounts. The records given in Tables 2 and 3 indicate that AgNP@AC Langmuir isotherms are observed to be linear throughout the entire concentration range and high correlation coefficients (R^2) are obtained. The high R^2 values indicate the applicability of the experimental data to the Langmuir model, which represents the single-layered adsorption (63). Furthermore, the separation factor, R_L obtained from recorded data according to Equation (4) ranges between 0 and 1. This indicates that the adsorption of AgNPs onto AC is favorable.

Also, the increase in qe with the increase in temperature confirms that the nature of their adsorption is endothermic, as mentioned above in the effect of temperature on adsorption. Since K_L constant is considered as an equilibrium constant in adsorption processes, an increase of K_L with temperature increases indicates that the equilibrium shifts to the right (Table 2) (64). Freundlich isotherm parameters such as K_F and n were obtained from the slope and intercept of the lnq_e–lnC_e linear plots shown in Fig. 6(b) (58). As R^2 values of Freundlich isotherms are lower than that of Langmuir isotherms, it is suggested that AgNP@AC adsorption does not fit the Freundlich isotherm model which suggests multilayered adsorption (57).

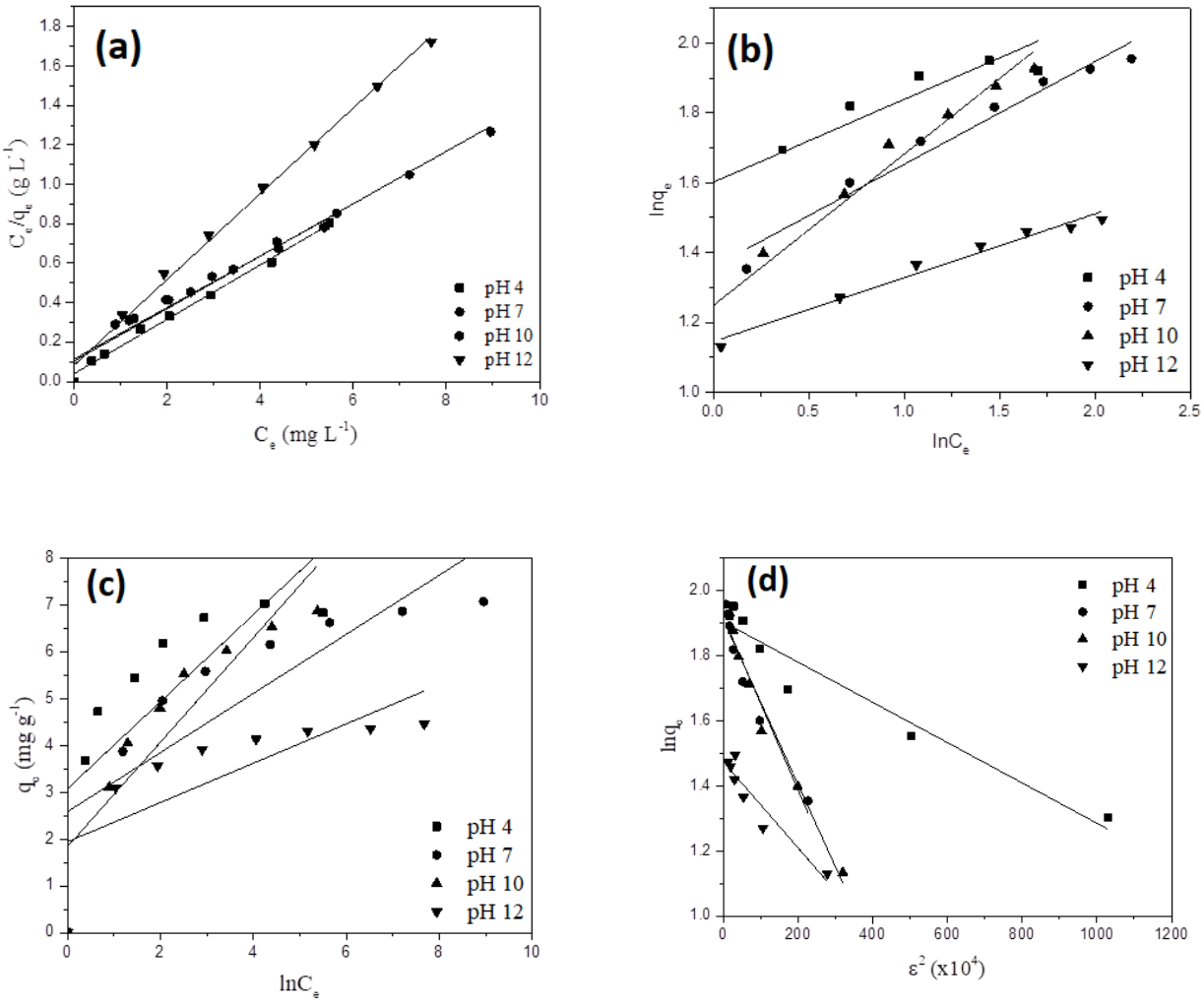

Figure 6: Isotherm plots of AgNP@AC adsorption (a) Langmuir, (b) Freundlich, (c) Temkin and (d) Dubinin–Radushkevich (AgNP concentration: 4–14 mg L^{-1}, pH: 4–12, AC dosage: 0.05 g, 298 K).

In the AgNP@AC adsorption study, the heat of adsorption and the interaction between adsorbent–adsorbate were evaluated using the Temkin isotherm. Temkin isotherm plots, shown in Figure 6(c), were obtained from the studies which were carried out at different pH values at 298 K. Temkin isotherm parameters, B and K_T were obtained from the slope and the intercept, respectively (58). The heat of adsorption is expected to decrease by increasing the temperature, and the reaction of adsorption takes place exothermically (64). From the results given in Tables 2 and 3, one can see that Temkin isotherm parameters increase as the temperature increases which suggests that the adsorption process is endothermic. It can be stated that the type of adsorption is physical adsorption involving electrostatic and Van der Waals interactions between AgNP and AC since the B values are less than 84 kJ mol^{-1} (54). But the high correlation coefficient (R^2) could not be obtained from Temkin isotherms. Therefore, those parameters obtained from Temkin isotherms cannot provide definite results for AgNP@AC adsorption.

Equilibrium adsorption data were fitted using D–R isotherm which suggests whether the AgNP@AC adsorption process is physical or chemical (61). This isotherm is more general than the Langmuir isotherm because there is no need to assume a hypothetical surface or a constant adsorption potential (65).

It is known that Langmuir and Freundlich isotherm constants do not give any idea for the adsorption mechanism. Consequently, equilibrium data were evaluated by D–R isotherm to understand the type of adsorption. By applying the experimental data to the D–R equation, the D–R isotherms at different pH values at 298 K are shown in Figure 6(d). K_{DR} and q_s D–R parameters were calculated from the slope and intercept of the plots, respectively (Tables 2 and 3) (59). E values (the mean free energy for adsorption)

were calculated using Equation (9) (61,65). E values for AgNP were found to be 1 – 8 kJ mol^{-1}. This reveals that the adsorption mechanism for AgNP@AC adsorption is physical. However, the R^2 values obtained from D–R isotherms are low, as, in Freundlich and Temkin isotherms, there is no definite conclusion about the AgNP@AC adsorption process from parameters obtained from D–R isotherms. According to the R^2 values obtained from various isotherms, it can be stated that the AgNP@AC adsorption process is defined best with the Langmuir model.

Thermodynamic Study

Thermodynamic parameters such as Gibbs free energy *(ΔG°),* enthalpy *(ΔH°),* and entropy *(ΔS°)* change were calculated from the equations given below to examine whether the adsorption process is endothermic or exothermic, and its behavior thermodynamically.

$$\Delta G^{\circ} = -RT \ln K_L \quad (11)$$

Where, R is the universal gas constant (8.314 J mol^{-1} K^{-1}), T absolute temperature (K), and K_L is the thermodynamic equilibrium constant. Negative ΔG° values indicate the feasibility and spontaneous occurrence of the adsorption process. The enthalpy *(ΔH°)* and entropy *(ΔS°)* changes are determined by the Van't Hoff equation given below.

$$lnK_L = \frac{\Delta S^{\circ}}{R} - \frac{\Delta H^{\circ}}{RT} \quad (12)$$

According to the equation, the lnK_L vs. $1/T$ graph was obtained and is shown in Figure 7. The thermodynamic parameters ΔH° and ΔS° are calculated from the slope and intercept, respectively (59). The calculated thermodynamic parameters are given in Table 4. The positive values of ΔH° indicate that AgNP@AC adsorption is endothermic. The positive values of the ΔS° values indicate the nano–silver affinity towards the activated carbon as well as the increased irregularity at the solid/solution interface during the adsorption process. The negative ΔG° values indicate the feasibility and spontaneity of the adsorption. In general, ΔG° of physical adsorption is lower than that of chemical adsorption. While the magnitude of physical adsorption varies between -20 – 0 kJ mol^{-1}, it is between -80 – -400 kJ mol^{-1} for chemical adsorption (66).

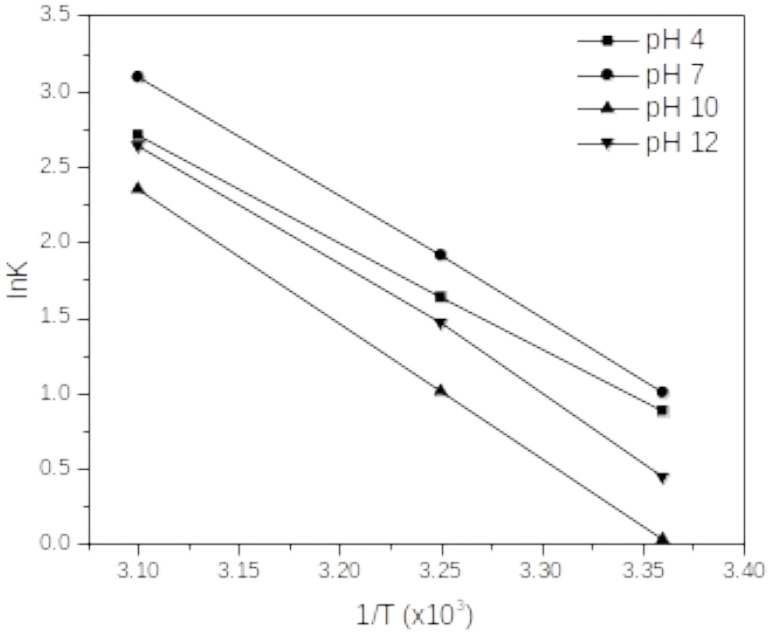

Figure 7: Van't Hoff plots for staining AgNP@AC adsorption at different pH values.

Also, the adsorption process can be classified to some extent by ΔH° as physical adsorption or chemical adsorption. A change of enthalpy <84 kJ mol^{-1} represents physisorption and values between 84 and 420 kJ mol^{-1} are considered (54).

Considering both the ΔG° and ΔH° values for the AgNP@AC adsorption process, it suggests that single layer adsorption occurs at different temperatures and conditions by means of a physical process.

Table 2: Isotherm parameters and correlation coefficients calculated by various isotherm models for AgNP@AC adsorption (AgNP concentration: 4–14 mgL^{-1}, pH: 4–12, AC dosage: 0.05 g, 298–323 K).

Isotherm	**Parameter**	**Value of parameters**											
		pH 4			**pH 7**			**pH 10**			**pH 12**		
	Temparature (K)	**298**	**308**	**323**	**298**	**308**	**323**	**298**	**308**	**323**	**298**	**308**	**323**
Langmuir	q_m *(mg* g^{-1}*)*	7.48	7.91	9.23	7.89	9.11	10.36	7.00	8.50	9.07	4.81	7.16	7.20
	K_L *(L* mg^{-1}*)*	2.42	5.14	15.04	2.74	6.79	22.11	1.03	2.76	4.35	1.56	10.51	14.00
	R^2	0.08 0.997	0.02 0.999	0.02 0.999	0.04 0.997	0.01 0.999	0.02 0.999	0.12 0.997	0.10 0.999	0.02 0.999	0.02 0.999	0.04 0.999	0.12 0.999
Freundlich	K_F *(L* mg^{-1}*)*	4.96	6.02	7.91	3.88	7.84	9.42	3.48	5.43	7.64	3.14	5.4	6.1
	N	4.21	5.4	8.64	3.4	7.18	8.12	2.3	4.13	8.26	5.46	543	8.53
	R^2	0.942	0.907	0.845	0.966	0.965	0.953	0.972	0.984	0.975	0.978	0.864	0.836
Temkin	B	1.258	1.083	0.826	1.596	0.885	0.885	2.203	1.422	0.805	0.690	0.996	0.679
	K_T *(L* mg^{-1}*)*	57.15	300	17206	10.42	8134	64263	1.275	50.19	15656	91.1	251	9200
	b_T	1969	2364	3251	1552	2893	3034	1178	1801	3336	3590	2571	3950
	R^2	0.961	0.940	0.890	0.989	0.956	0.985	0.995	0.998	0.992	0.987	0.899	0.862
D-R	q_s *(mg* g^{-1}*)*	6.72	7.45	9.05	1.916	8.13	9.66	6.68	7.32	8.31	4.34	6.84	7.1
	K_{DR} *(*mol^2 J^2*)*	6.E-08	3.E-08	1.E-08	3.E-07	5.E-09	5.E-09	2.E-07	6.E-08	7.E-09	1.E-07	5.E-08	2.E-08
	E *(kJ* mol^{-1}*)*	2.9	4.0	7.1	1.3	1.5	1.7	2.2	2.9	7.45	2.2	3.2	5.0
	R^2	0.946	0.902	0.997	0.947	0.813	0.967	0.9629	0.916	0.922	0.927	0.989	0.988

Table 3: Isotherm parameters and correlation coefficients calculated by various isotherm models for AgNP@AC adsorption (AgNP concentration: 4–14 mgL^{-1}, pH: 4–12, AC dosage: 0.01–0.03–0.05 g, 298 K).

Isotherm	**Parameter**	**Value of parameters**											
		pH 4			**pH 7**			**pH 10**			**pH 12**		
	Adsorbent (g)	**0.01**	**0.03**	**0.05**	**0.01**	**0.03**	**0.05**	**0.01**	**0.03**	**0.05**	**0.01**	**0.03**	**0.05**
Langmuir	q_m *(mg* g^{-1}*)*	10.52	9.52	7.48	10.73	9.91	7.89	10.33	9.84	7.00	7.49	6.63	4.81
	K_L *(L* mg^{-1}*)*	2.82	2.29	2.42	1.02	1.21	2.74	0.71	0.94	1.03	0.30	0.65	1.56
	R_L	0.03	0.04	0.08	0.05	0.08	0.04	0.12	0.10	0.12	0.31	0.19	0.12
	R^2	0.998	0.999	0.997	0.999	0.999	0.997	0.999	0.999	0.997	0.999	0.999	0.999
Freundlich	K_F *(L* mg^{-1}*)*	7.26	0.71	4.96	7.68	0.75	3.88	7.60	7.70	3.48	2.10	6.01	3.14
	N	3.52	6.46	4.21	3.99	5.86	3.4	7.10	4.82	2.3	2.16	28.25	5.46
	R^2	0.931	0.988	0.942	0.972	0.965	0.966	0.992	0.961	0.972	0.983	0.980	0.978
Temkin	B	1.938	2.032	1.258	1.722	1.134	1.596	0.949	1.389	2.203	1.797	0.187	0.690
	K_T *(L* mg^{-1}*)*	49.1	32.05	57.15	101.3	1819	10.42	3557	296.5	1.275	2.45	1.E+14	91.1
	b_T	1278	1219	1969	1439	2185	1552	3610	1784	1178	1379	13249	3590
	R^2	0.978	0.973	0.961	0.993	0.992	0.989	0.996	0.990	0.995	0.999	0.965	0.987
D-R	q_s *(mg* g^{-1}*)*	11.52	9.25	6.72	9.24	8.96	1.92	8.40	8.86	6.68	5.24	6.17	4.34
	K_{DR} *(mol²* J^2*)*	5.E-08	6.E-08	6.E-08	3.E-08	9.E-09	3.E-07	9.E-09	2.E-08	2.E-07	6.E-07	6.E-10	1.E-07
	E *(kJ* mol^{-1}*)*	3.16	6.24	2.9	6.67	7.45	1.3	5.45	5.00	2.20	0.91	1.87	2.20
	R^2	0.981	0.984	0.946	0.946	0.939	0.947	0.879	0.952	0.9629	0.956	0.871	0.927

Table 4: Thermodynamic parameters for AgNP@AC adsorption (AgNP concentration: 4–14 mg L^{-1}, pH: 4–12, AC dosage: 0.05 g).

pH	K_L	T (K)	ΔG° (kJ mol^{-1})	ΔH° (kJ mol^{-1})	ΔS° ($Jmol^{-1}$ K^{-1})	R^2
4	2.42	298	-2.19	58.53	203.70	0.9999
	5.14	308	-4.19			
	15.04	323	-7.28			
7	2.74	298	-2.49	66.77	232.92	0.9970
	6.79	308	-4.50			
	22.11	323	-8.31			
10	1.03	298	-0.08	74.21	249.33	0.9999
	2.76	308	-2.59			
	10.51	323	-6.32			
12	1.56	298	-1.11	69.78	328.35	0.9971
	4.35	308	-3.77			
	14.00	323	-7.09			

CONCLUSION

AgNPs were synthesized by using gelatin as a capping agent. Colloidal stability of AgNPs was checked at pHs of 2–13. AgNPs displayed colloidal stability at pHs ranging from 4 to 13. The stability of the nanoparticles was observed to weaken at a pH of 2. AgNP adsorption onto AC was examined and found to be influenced by experimental parameters including initial nanoparticle concentration, temperature, pH, and adsorbent dosage. Adsorption percentage decreased with increased initial nanoparticle concentration. However, qe value seemed to increase per AC mass as nanoparticle concentration increased. Temperature increase promoted AgNP adsorption onto AC. The amount of adsorbed AgNP per unit mass of AC decreases as adsorbent dosage increases. Adsorption isotherms were investigated by fitting the data to different isotherm models including Langmuir, Freundlich, Temkin, and Dubinin–Radushkevich (D–R). Results suggest that the adsorption is well described by the Langmuir model. Thermodynamic studies indicated that the adsorption is endothermic, favorable, and spontaneous. Our findings reveal that gelatin–stabilized AgNPs can be successfully removed from water using AC.

CONFLICT OF INTEREST

Authors declare that they have no conflict of interest.

ACKNOWLEDGMENTS

The authors gratefully thank Karabük University for the support by a grant from the [Project 16/1-DS-245].

REFERENCES

1. García-Barrasa J, López-De-luzuriaga JM, Monge M. Silver nanoparticles: Synthesis through chemical methods in solution and biomedical applications. Cent Eur J Chem. 2011;9(1):7–19. <DOI>.

2. Calderón-Jiménez B, Johnson ME, Montoro Bustos AR, Murphy KE, Winchester MR, Baudrit JRV. Silver nanoparticles: Technological advances, societal impacts, and metrological challenges. Front Chem. 2017;5(Feb):1–26. <DOI>.

3. Sivera M, Kvitek L, Soukupova J, Panacek A, Prucek R, Vecerova R, et al. Silver nanoparticles modified by gelatin with extraordinary pH stability and long-term antibacterial activity. PLoS One. 2014;9(8). <DOI>.

4. Seoudi R, Shabaka A, El Sayed ZA, Anis B. Effect of stabilizing agent on the morphology and optical properties of silver nanoparticles. Phys E Low-Dimensional Syst Nanostructures. 2011;44(2):440–7. <DOI>.

5. Alarcon EI, Bueno-Alejo CJ, Noel CW, Stamplecoskie KG, Pacioni NL, Poblete H, et al. Human serum albumin as protecting agent of silver nanoparticles: Role of the protein conformation and amine groups in the nanoparticle stabilization. J Nanoparticle Res. 2013;15(1). <DOI>.

6. Salgueiriño-Maceira V, Correa-Duarte MA, Farle M, López-Quintela MA, Sieradzki K, Diaz R. Synthesis and characterization of large colloidal cobalt particles. Langmuir. 2006;22(4):1455–8. <DOI>.

7. Campos AM, Raymundo-Pereira PA, Cincotto FH, Canevari TC, Machado SAS. Sensitive determination of the endocrine disruptor bisphenol

A at ultrathin film based on nanostructured hybrid material SiO2/GO/AgNP. J Solid State Electrochem. 2016;20(9):2503–7. <DOI>.

8. Mdluli PS, Revaprasadu N. An improved N,N-dimethylformamide and polyvinyl pyrrolidone approach for the synthesis of long silver nanowires. J Alloys Compd. 2009;469(1–2):519–22. <DOI>.

9. Kashiwagi Y, Yamamoto M, Nakamoto M. Facile size-regulated synthesis of silver nanoparticles by controlled thermolysis of silver alkylcarboxylates in the presence of alkylamines with different chain lengths. J Colloid Interface Sci. 2006;300(1):169–75. <DOI>.

10. Brust M, Kiely CJ. Some recent advances in nanostructure preparation from gold and silver particles: A short topical review. Colloids Surfaces A Physicochem Eng Asp. 2002;202(2–3):175–86. <DOI>.

11. Bunge SD, Boyle TJ, Headley TJ. Synthesis of coinage-metal nanoparticles from mesityl precursors. Nano Lett. 2003;3(7):901–5. <DOI>.

12. Pastoriza-Santos I, Liz-Marzán LM. Formation of PVP-protected metal nanoparticles in DMF. Langmuir. 2002;18(7):2888–94. <DOI>.

13. Ahmad M Bin, Lim JJ, Shameli K, Ibrahim NA, Tay MY. Synthesis of silver nanoparticles in chitosan, gelatin and chitosan/gelatin bionanocomposites by a chemical reducing agent and their characterization. Molecules. 2011;16(9):7237–48. <DOI>.

14. Jia Z, Sun H, Gu Q. Preparation of Ag nanoparticles with triethanolamine as reducing agent and their antibacterial property. Colloids Surfaces A Physicochem Eng Asp. 2013;419:174–9. <DOI>.

15. Xiong Y, Luo G, Chen C, Yuan H, Shen Q, Li M. In situ synthesis of zero-valent silver nanoparticles in polymethylmethacrylate under high temperature. Appl Surf Sci. 2012;258(15):5822–6. <DOI>.

16. Sun X, Dong S, Wang E. One-step preparation and characterization of poly(propyleneimine) dendrimer-protected silver nanoclusters. Macromolecules. 2004;37(19):7105–8. <DOI>.

17. Long Y, Ran X, Zhang L, Guo Q, Yang T, Gao J, et al. A method for the preparation of silver nanoparticles using commercially available carboxymethyl chitosan and sunlight. Mater Lett. 2013;112:101–4. <DOI>.

18. Moussa SH, Tayel AA, Alsohim AS, Abdallah RR. Botryticidal activity of nanosized silver-chitosan composite and its application for the control of gray mold in strawberry. J Food Sci. 2013;78(10):1589–94. <DOI>.

19. Oluwafemi OS, Lucwaba Y, Gura A, Masabeya M, Ncapayi V, Olujimi OO, et al. A facile completely “green” size tunable synthesis of maltose-reduced silver nanoparticles without the use of any accelerator. Colloids Surfaces B Biointerfaces. 2013;102:718–23. <DOI>.

20. Lee C, Zhang P. Facile synthesis of gelatin-protected silver nanoparticles for SERS applications. J Raman Spectrosc. 2013;44(6):823–6. <DOI>.

21. Darroudi M, Khorsand Zak A, Muhamad MR, Huang NM, Hakimi M. Green synthesis of colloidal silver nanoparticles by sonochemical method. Mater Lett. 2012;66(1):117–20. <DOI>.

22. Zamiri R, Azmi BZ, Ahangar HA, Zamiri G, Husin MS, Wahab ZA. Preparation and characterization of silver nanoparticles in natural polymers using laser ablation. Bull Mater Sci. 2012;35(5):727–31. <DOI>.

23. Cushing BL, Kolesnichenko VL, O’Connor CJ. Recent advances in the liquid-phase syntheses of inorganic nanoparticles. Chem Rev. 2004;104(9):3893–946. <DOI>.

24. Evanoff DD, Chumanov G. Synthesis and optical properties of silver nanoparticles and arrays. ChemPhysChem. 2005;6(7):1221–31.<DOI>.

25. Valdés H, Sánchez-Polo M, Rivera-Utrilla J, Zaror CA. Effect of ozone treatment on surface properties of activated carbon. Langmuir. 2002;18(6):2111–6. <DOI>.

26. Fabris D, Garg V, Sapag K, Oliveira LCA, Rios RVRA, Lago RM. Activated carbon / iron oxide magnetic composites for the adsorption of contaminants in water. 2002;40:2177–83. <DOI>.

27. Eltugral N, Simsir H, Karagoz S. Preparation of nano-silver-supported activated carbon using different ligands. Res Chem Intermed. 2016;42(3):1663–76.<DOI>.

28. Panáček A, Kvítek L, Prucek R, Kolář M, Večeřová R, Pizúrová N, et al. Silver colloid nanoparticles: Synthesis, characterization, and their antibacterial activity. J Phys Chem B. 2006;110(33):16248–53. <DOI>.

29. Boehm HP. Chemical Identification of Surface Groups. Adv Catal. 1966;16(C):179–274. <DOI>.

30. Teng H, Xu S, Zhao C, Lv F, Liu H. Removal of Hexavalent Chromium from Aqueous Solutions by Sodium Dodecyl Sulfate Stabilized Nano Zero-Valent Iron: A Kinetics, Equilibrium, Thermodynamics Study. Sep Sci Technol. 2013;48(11):1729–37. <DOI>.

31. Maity D, Kanti Bain M, Bhowmick B, Sarkar J, Saha S, Acharya K, et al. In situ synthesis, characterization, and antimicrobial activity of silver nanoparticles using water soluble polymer. J Appl Polym Sci. 2011;122(4):2189–96. <DOI>.

32. Srinivasan NR, Shankar PA, Bandyopadhyaya R. Plasma treated activated carbon impregnated with silver nanoparticles for improved antibacterial effect in water disinfection. Carbon N Y. 2013;57(22):1–10. <DOI>.

33. Peña-González CE, Pedziwiatr-Werbicka E, Shcharbin D, Guerrero-Beltrán C, Abashkin V, Loznikova S, et al. Gold nanoparticles stabilized by cationic carbosilane dendrons: Synthesis and biological properties. Dalt Trans. 2017;46(27):8736–45.<DOI>.

34. El-Shishtawy RM, Asiri AM, Al-Otaibi MM. Synthesis and spectroscopic studies of stable aqueous dispersion of silver nanoparticles. Spectrochim Acta - Part A Mol Biomol Spectrosc. 2011;79(5):1505–10. <DOI>.

35. Ho CM, Yau SKW, Lok CN, So MH, Che CM. Oxidative dissolution of silver nanoparticles by biologically relevant oxidants: A kinetic and mechanistic study. Chem - An Asian J. 2010;5(2):285–93. <DOI>.

36. Dickinson E, Lopez G. Comparison of the emulsifying properties of fish gelatin and commercial milk proteins. J Food Sci. 2001;66(1):118–23. <DOI>.

37. Hashim DM, Man YBC, Norakasha R, Shuhaimi M, Salmah Y, Syahariza ZA. Potential use of Fourier transform infrared spectroscopy for differentiation of bovine and porcine gelatins. Food Chem. 2010;118(3):856–60.<DOI>.

38. Solanki PR. Gelatin Nanoparticles as a Delivery System for Proteins. J Nanomedicine Res. 2015;2(1):2–4.<DOI>.

39. Shende S, Ingle AP, Gade A, Rai M. Green synthesis of copper nanoparticles by Citrus medica Linn. (Idilimbu) juice and its antimicrobial activity. World J Microbiol Biotechnol. 2015;31(6):865–73.<DOI>.

40. Usman MS, El Zowalaty ME, Shameli K, Zainuddin N, Salama M, Ibrahim NA. Synthesis, characterization, and antimicrobial properties of copper nanoparticles. Int J Nanomedicine. 2013;8:4467–79. <DOI>.

41. Pandey S, Goswami GK, Nanda KK. Green synthesis of biopolymer-silver nanoparticle nanocomposite: An optical sensor for ammonia detection. Int J Biol Macromol. 2012;51(4):583–9.<DOI>.

42. Wang X, Chen Y. A new two-phase system for the preparation of nearly monodisperse silver nanoparticles. Mater Lett. 2008;62(28):4366–8. <DOI>.

43. Das D, Samal DP, BC M. Preparation of Activated Carbon from Green Coconut Shell and its Characterization. J Chem Eng Process Technol. 2015;06(05).<DOI>.

44. Tuan TQ, Son N Van, Dung HTK, Luong NH, Thuy BT, Anh NT Van, et al. Preparation and properties of silver nanoparticles loaded in activated carbon for biological and environmental applications. J Hazard Mater. 2011;192(3):1321–9. <DOI>.

45. Karthik C, Radha K V. Silver nanoparticle loaded activated carbon: An escalated nanocomposite with antimicrobial property. Orient J Chem. 2016;32(1):735–41. <DOI>.

46. Chun Y, Sheng G, Chiou GT, Xing B. Compositions and sorptive properties of crop residue-derived chars. Environ Sci Technol. 2004;38(17):4649–55. <DOI>.

47. Ridder DJ de. Adsorption of organic micropollutants onto activated carbon and zeolites. Vol. P.hD, Water management academic press. 2012. <DOI>.

48. Senthilkumaar S, Varadarajan PR, Porkodi K, Subbhuraam C V. Adsorption of methylene blue onto jute fiber carbon: Kinetics and equilibrium studies. J Colloid Interface Sci. 2005;284(1):78–82. <DOI>.

49. Zhu HY, Fu YQ, Jiang R, Jiang JH, Xiao L, Zeng GM, et al. Adsorption removal of congo red onto magnetic cellulose/Fe3O4/activated carbon composite: Equilibrium, kinetic and thermodynamic studies. Chem Eng J. 2011;173(2):494–502. <DOI>.

50. Ghaedi M, Sadeghian B, Pebdani AA, Sahraei R, Daneshfar A, Duran C. Kinetics, thermodynamics and equilibrium evaluation of direct yellow 12 removal by adsorption onto silver nanoparticles loaded activated carbon. Chem Eng J. 2012;187:133–41. <DOI>.

51. Garg VKKR, Gupta R. Dyes Pigments. Remov malachite green Dye from aqueous Solut by Adsorpt using agro-industry waste a case study Prosopis cineraria. 2004;62:1–10. <DOI>.

52. Honeyman BD, Santschi PH. Metals in aquatic systems. Environ Sci Technol. 1988;22(8):862–71.<DOI>.

53. Manohar DM, Anoop Krishnan K, Anirudhan TS. Removal of mercury(II) from aqueous solutions and chlor-alkali industry wastewater using 2-mercaptobenzimidazole-clay. Water Res. 2002;36(6):1609–19. <DOI>.

54. Al-Degs YS, El-Barghouthi MI, El-Sheikh AH, Walker GM. Effect of solution pH, ionic strength, and temperature on adsorption behavior of reactive dyes on activated carbon. Dye Pigment. 2008;77(1):16–23. <DOI>.

55. Norde W, Lyklema J. Thermodynamics of protein adsorption. Theory with special reference to the adsorption of human plasma albumin and bovine pancreas ribonuclease at polystyrene surfaces. J Colloid Interface Sci. 1979;71(2):350–66.<DOI>.

56. Bhatnagar A, Sillanpää M. Removal of natural organic matter (NOM) and its constituents from water by adsorption – A review. Chemosphere. 2017;166:497–510. <DOI>.

57. Jalil AA, Triwahyono S, Adam SH, Rahim ND, Aziz MAA, Hairom NHH, et al. Adsorption of methyl orange from aqueous solution onto calcined Lapindo volcanic mud. J Hazard Mater. 2010;181(1–3):755–62. <DOI>.

58. Ng C, Losso JN, Marshall WE, Rao RM. Freundlich adsorption isotherms of agricultural by-product-based powdered activated carbons in a geosmin-water system. Bioresour Technol. 2002;85(2):131–5. <DOI>.

59. Da A. Adsorption- from theory to practice. 2001;93(1–3):135–224. <DOI>.

60. Foo KY, Hameed BH. Insights into the modeling of adsorption isotherm systems. Chem Eng J. 2010;156(1):2–10. <DOI>.

61. Sogut E, Caliskan N. Isotherm and kinetic studies of Pb(II) adsorption on raw and modified diatomite by using non-linear regression method. Fresenius Environ Bull. 2017;26(4):2721–9. <DOI>.

62. Günay A, Arslankaya E, Tosun I. Lead removal from aqueous solution by natural and pretreated clinoptilolite: Adsorption equilibrium and kinetics. J Hazard Mater. 2007;146(1–2):362–71. <DOI>.

63. Özer A, Özer D, Özer A. The adsorption of copper(II) ions on to dehydrated wheat bran (DWB): Determination of the equilibrium and thermodynamic parameters. Process Biochem. 2004;39(12):2183–91. <DOI>.

64. Nekouei F, Nekouei S, Tyagi I, Gupta VK. Kinetic, thermodynamic and isotherm studies for acid blue 129 removal from liquids using copper oxide nanoparticle-modified activated carbon as a novel adsorbent. J Mol Liq. 2015;201:124–33.<DOI>.

65. Kilislioglu A, Bilgin B. Thermodynamic and kinetic investigations of uranium adsorption on amberlite IR-118H resin. Appl Radiat Isot. 2003;58(2):155–60. <DOI>.

66. Weil KG. M. J. Jaycock, G. D. Parfitt: Chemistry of Interfaces. Ellis Horwood Limited Publishers, Chichester 1981. Berichte der Bunsengesellschaft für Phys Chemie. 1981;85(9):718–718.<DOI>.

SUPPLEMENTARY MATERIAL

Isotherm and Thermodynamic Studies on the Removal of Gelatin-stabilized Silver Nanoparticles from Water by Activated Carbon

Aysenur Ceryan[1], Nurettin Eltugral[2*]

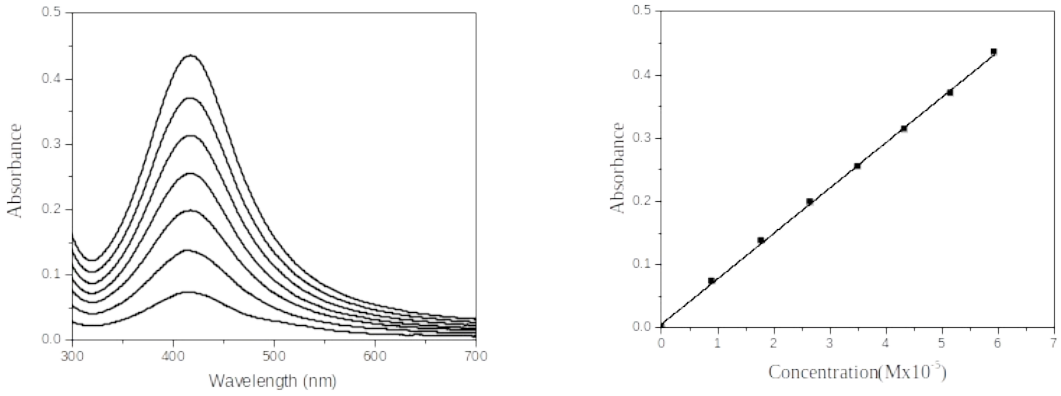

(a) (b)

Figure S1: UV-Vis absorbance spectra and b) Lambert-Beer plot of AgNP solutions at different concentrations (9.0×10^{-6} - 6.0×10^{-5} M).

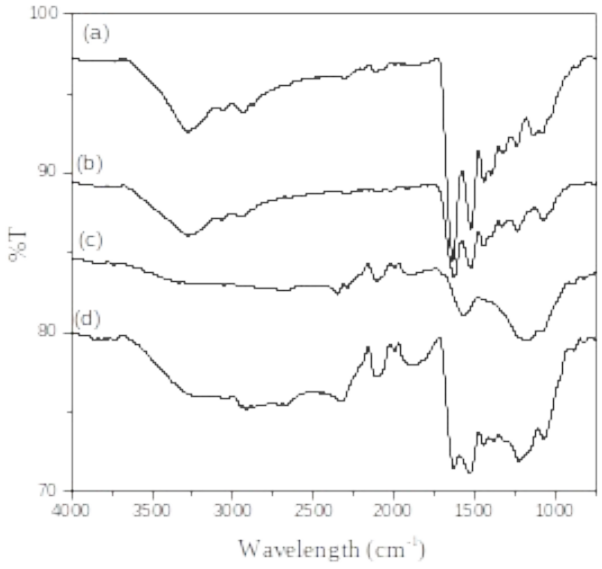

Figure S2: FTIR spectrum of a) Gelatin, b) AgNP, c) AC, and d) AgNP@AC

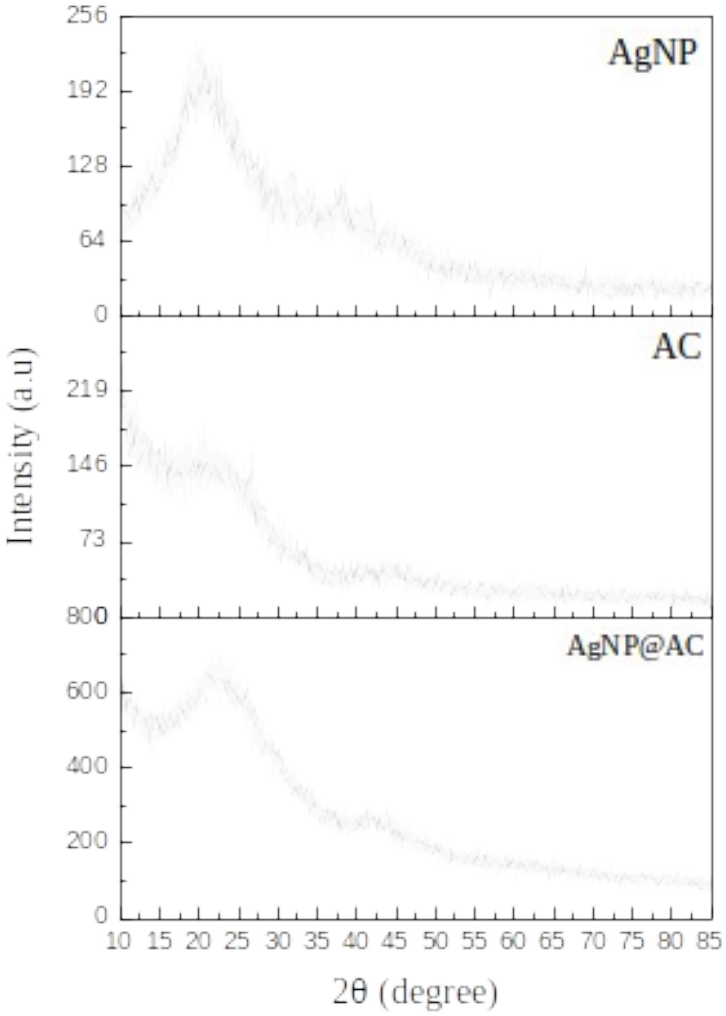

Figure S3: XRD diffraction patterns of AgNP, AC, and AgNP@AC.